Plasma and fluidic jet actuators for circulation control around wind turbulne airfoils

A. Leroy, C. Braud, V. Jaunet, S. Baleriola, Emmanuel Guilmineau, T. Piquet, S. Loyer, Philippe Devinant, Sandrine Aubrun

52nd 3AF International Conference on Applied Aerodynamics
27 – 29 March 2017, Lyon - France

FP05-AERO2017-Leroy

PLASMA AND FLUIDIC JET ACTUATORS FOR CIRCULATION CONTROL AROUND WIND TURBINE AIRFOILS

A. Leroy[(1)], C. Braud[(2)], V. Jaunet[(2)], S. Baleriola[(1)], E. Guilmineau[(2)], T. Piquet[(2)], S. Loyer[(1)], P. Devinant[(1)], S. Aubrun[(1)]

[(1)] Université d'Orléans, PRISME, EA 4229, F-45072, Orléans, France, Email: annie.leroy@univ-orleans.fr
[(2)] LHEEA, Ecole Centrale Nantes, F-44321 Nantes Cedex 3, France, Email: caroline.braud@ec-nantes.fr

ABSTRACT

In order to reduce the aerodynamic load fluctuations on wind turbine blades by innovative control solutions, strategies of active circulation control acting at the blade airfoil trailing edge are studied. This paper focuses on a comparison of results obtained by performing plasma and continuous squared jet actuation experimentally and slotted jet actuation numerically on a blade airfoil designed with a rounded trailing edge. Plasma actuators and slotted jets act uniformly in the spanwise direction (two-dimensional action), whereas squared jets blow through small squared holes distributed along the span, and therefore, provide a three-dimensional action on the flow. Results are presented for a chord Reynolds number of $2x10^5$. Time averaged aerodynamic values, flow fields were analysed to assess the effectiveness of these actuators located at the rounded trailing edge and to highlight flow mechanisms involved in this type of flow control strategy.

1. INTRODUCTION

Due to inhomogeneous and unsteady incoming wind conditions, it is expected that wind turbine airfoils under real operating conditions may encounter variation of ± 5° around in angles of attack, inducing load variations to mitigate. It is then necessary to optimize the wind energy efficiency and the rotor lifetime by developing innovative control concepts with the intention of reducing load fluctuations on blades.

Strategies of circulation control acting at the airfoil trailing edge are usually investigated to allow lift increase and decrease. For aerodynamic bodies they are traditionally implemented by means of concepts including shape change, flaps, blowing, suction, etc., and often make use of the Coanda effect that keeps a tangential jet attached over a curved surface, but it is usually necessary for conventional blowing to be characterized by a high momentum coefficient, as exposed in [1] or [2]. Recent applications are turned nowadays towards wind turbines [3-4] and water turbines.

This work aims at investigating experimentally the potentialities of two unconventional methods of circulation control to reduce load fluctuations. Two types of actuators are used in this circulation control application, dielectric barrier discharges (DBD) as surface plasma actuators (PA) and squared jet distribution (SJD). Both actuators are characterized by quite low momentum coefficients and allow to perform a bi-dimensional and a three-dimensional action on the flow, respectively. It is assumed that the flow induced by the DBD actuator behaves like a two-dimensional wall jet whereas jets do not act uniformly in the spanwise direction since they are discretely distributed and therefore provide a three-dimensional action. Interest in plasma actuators for flow control has been largely reported in the literature over the last decade. Recent studies have dealt with control circulation by surface plasma actuators [5-6] in which the feasibility of this strategy was demonstrated. Continuous fluidic jet distribution are more conventionally used for turbulent boundary layer separation control. Indeed, when fluidic round jets are inclined relatively to the wall and to the main stream of the baseline flow, they are able to generate streamwise vortices qualitatively similar to those of passive vortex generators [7-8]. By comparing slotted jet control and discrete round jet control, experimentally and numerically on the same configuration [9-10], it was found that the most efficient control is obtained when the structures resulting from the interaction of the control jet with the cross-flow (streamwise or spanwise), have a long enough coherence to reinforce the turbulent boundary subjected to an adverse pressure gradient.

As a first stage, the objective of this study is to assess the potentialities of different circulation control techniques by conducting experimental and numerical investigations

in open-loop approach. The baseline aerodynamic configuration is a fully attached flow on the airfoil, and the final objective of the control is to maintain the lift at a fixed value, whatever the incoming flow disturbances. Load and velocity field measurements were performed to assess the effectiveness of actuators and to highlight the flow mechanisms induced by both experimental actuation methods for lift-up configurations. The numerical approach was first based on 2D URANS simulations performed with the flow solver ISIS-CFD in which slotted jets are modelled. Results are presented in terms of lift gain variation according to momentum coefficients and modifications observed in the topology of the near wake.

2. CIRCULATION CONTROL ORIENTED AIRFOIL MODEL

In order to enable a circulation control of an attached flow around an airfoil, it is necessary to make the trailing edge round. For this study, the trailing edge of the generic NACA654- 421 profile was replaced by a rounded one with a radius of curvature of 2% of the chord. The shape adjustment between the modified trailing edge and the pressure side was designed in order to increase the airfoil camber, as a compensation for the expected degradation of the drag due to the thickening of the trailing edge. Figure 1 shows the comparison between the generic NACA654-421 airfoil profile and the CC-oriented airfoil profile NACA654-421-CC. More details on aerodynamic performances are described in [11].

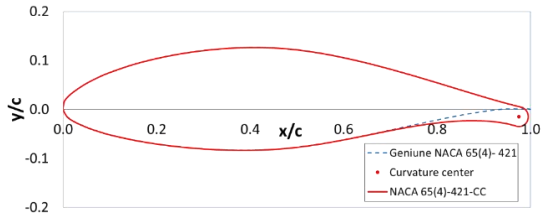

Figure 1. Section view of the control circulation oriented NACA65$_4$-421-CC.

3. EXPERIMENTAL AND NUMERICAL SIMULATION SET UP

3.1. Description of experimental equipment

The experiments were carried out at the closed return wind tunnel of the PRISME laboratory. Two airfoils having the NACA654-421-CC profile were specifically designed respectively for PA or SJD purposes. They had a chord of c = 300mm and a wing span of 1.1m. The airfoils were then mounted horizontally between two vertical flat planes in order to achieve a 2D flow configuration into the 5m long main test section with a cross-section of 2m × 2m. They were mounted on both tips onto a balance used for time-averaged lift and drag measurements and located under the test section. The balance was carefully calibrated, lift and drag coefficient uncertainties were estimated at 10m/s to be less than 5% for the lift force and 10% for the drag force. In the present study, the operating speed of the wind tunnel is 10m/s with an airflow turbulence level below 0.4%. In this study, results will be presented for a Reynolds number of 2.10^5.

Mean pressure distribution around the airfoil was measured with pressure taps implemented around the model. 20 pressure taps are available for the PA airfoil in the median section. For the SJD airfoil, 42 pressure taps are distributed chordwise. The airfoil was designed so that each pressure tap can be either used as micro-jet or as a pressure tap. Several orifices can be found at each chord location in the spanwise direction and are connected to the same plenum chamber. Pressure measurement values are then the result of a space-average in the transverse direction. Mean velocity fields around the airfoil trailing edge were studied from 2D-PIV measurements in order to analyse flow topology in streamwise planes of the airfoil model and more particularly in the median plane (z = 0mm). The PIV system consisted, in the case of the wind-tunnel experiments, in a Nd:Yag laser (2 × 200mJ) emitting pulses with a 2.5Hz emission rate. The light sheet was oriented in order to visualize simultaneously both pressure and suction sides of the airfoil. Seeding particles were micro-sized olive oil droplets sprayed by a PIVTEC seeding system. Images were acquired with a LaVision Imager LX camera (4032px × 2688px) and a 200mm lens. 1,000 image pairs were recorded. For SJD configuration, vector fields were computed using OpenPIV Software running in parallel [12]. A signal to noise ratio of 1.3 and a threshold filter on velocity components were used to validate the vector field. The final resolution is of one vector every 0.8mm with a 32px × 32px interrogation window. For PA, images processing was carried out with DaVis 8.3 LaVision software and the final resolution is of one vector every 0.4mm with a 32px × 32px interrogation window with an overlap of 50%. For the quiescent air experiments, the same seeding system was used as well as a similar laser. The camera used was a TSI Power View (2048px × 2048px) with a 200 mm lens. 600 image pairs were recorded for every configuration. This system allows a final resolution of one vector every 0.5mm with a 32px × 32px interrogation window.

3.2. Plasma actuators

Fig. 2 shows the section view of the trailing edge airfoil section equipped with the PA made of two successive single DBD. One single DBD consists in two copper electrodes that are positioned on both sides of a dielectric material (PMMA, 3 mm thick) of the model cap. The

high voltage electrodes (or active electrodes) are serrated and powered with an AC-power supply up to 18kV and 1kHz, while the grounded one is linear and encapsulated within the dielectric material of the model itself. The high voltage and grounded electrodes were 950mm long, while the length of the floating electrode was 900mm. With a high voltage application at the active electrode, the ambient air is ionized and accelerated, creating an ionic wind along the grounded electrode that permits the manipulation of the flow near the wall zone. Plasma is generated from the first high voltage electrode. For such an actuator, the electrical power consumption was measured and estimated at around 80 W/m. It is assumed that the flow induced by this actuator behaves like a two-dimensional wall jet. It was characterized in quiescent air conditions by PIV in the median airfoil section. As shown in Fig. 3, the ambient air is deflected towards the plasma region with an acceleration close to the wall, highlighting the higher velocity at the plasma-gas interface along the whole actuator. Downstream of the main actuation zone, one can observe diffusion of the induced jet on the normal direction to the wall. The velocity vector profiles suggest that the wall jet expands away from the wall because of the curvature resulting in a widened jet in the pressure side zone with slight lower streamwise velocities.

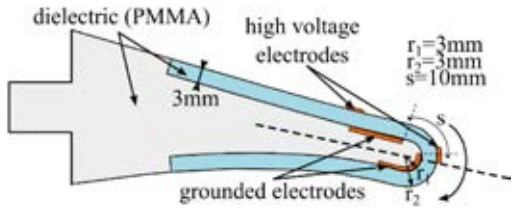

Figure 2. Scheme of the trailing edge equipped with the DBD actuator.

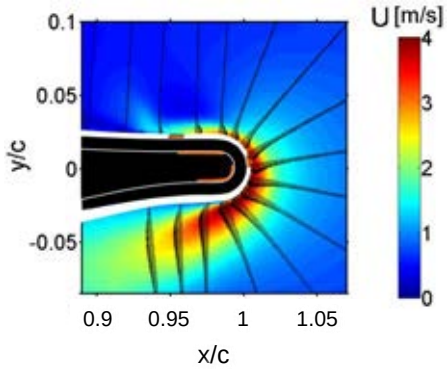

Figure 3. Time averaged magnitude velocity contours and velocity vector profiles of the flow induced by the DBD actuator (18 kV, 1 kHz).

The momentum coefficient C_μ, the typical figure of merit for discussing the circulation control efficiency, has been estimated. It was chosen to estimate the momentum coefficient by integration of the tangential velocity profile in the wall normal direction, in the plasma region, just at the downstream edge of the second grounded electrode, as done in [5] or [13].

$$C_\mu = \frac{\int_0^\infty \rho u^2(y)\, dy}{\frac{1}{2}\rho_\infty U_\infty^2 c} \quad (1)$$

Based on these results, for a freestream flow of U_∞ = 10 m/s, within this work, C_μ was about 0.004.

3.3. Continuous squared jets

Fig. 4 shows the section view of the trailing edge airfoil median (z = 0 mm) section equipped with one of the fluidic jet orifices supplied with air from both ends of the airfoil. The airfoil is equipped with a spanwise distribution of 42 SJD located at *x*/c = 0.96 and spaced by λ = 21 mm. The squared hole area is S_{jet} = 1 mm².

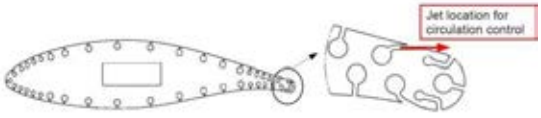

Figure 4. Fluidic jet orifice scheme close to the trailing edge.

The air system used to provide pressurized air to the actuators is composed of a compressor, a filtration system and a proportional valve. The momentum coefficient is derived from equation (2):

$$C_\mu = \frac{\rho_{jet} Q_v U_{jet}}{\frac{1}{2}\rho_\infty U_\infty^2 S} \quad (2)$$

where S = chord × span. Eq. (2) can be expressed in terms of the more practical total and static variables of the microjet [14] :

$$C_\mu = \frac{2\gamma M_{jet}^2}{\rho_\infty U_\infty^2} P_0 \left[1 + \frac{\gamma-1}{2} M_{jet}^2\right]^{-\gamma/(\gamma-1)} \frac{S_{jet}}{S} \quad (3)$$

where M_{jet} is the microjet Mach number, which can be obtained from the ratio of total to exit static pressure of the microjet, and P_0 is the microjet total pressure which can be easily measured in the plenum chamber of the microjet. The jet was characterized in quiescent air conditions using a laboratory-made total pressure (p_t) probe with an external diameter of 500µm and an inner diameter of 250µm ± 50 µm. It was placed on a 3D micro-displacement system with its axis in the streamwise direction. The probe was connected to a Furness manometer through Tygon tubes. Considering its velocity during those specific tests, the flow at the exit of the controlled jet can reasonably be assumed incompressible, so that the reference static pressure is

equal to the ambient pressure (p_0) and the jet exit speed is obtain using:

$$U_{jet} = \sqrt{\frac{2(p_t - p_0)}{\rho}} \quad (4)$$

The mean spatial topology of a single jet was investigated in the vertical (y) (see Fig. 5) and in the spanwise (z) (see Fig. 6) direction at different streamwise positions (x/c) in the median airfoil section, x/c = 1 corresponding to the position of the trailing edge end (see Fig. 1).

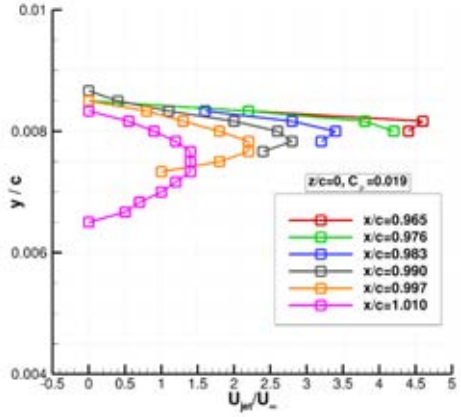

Figure 5. Streamwise velocity profiles as a function of the vertical position y/c at different streamwise positions x/c.

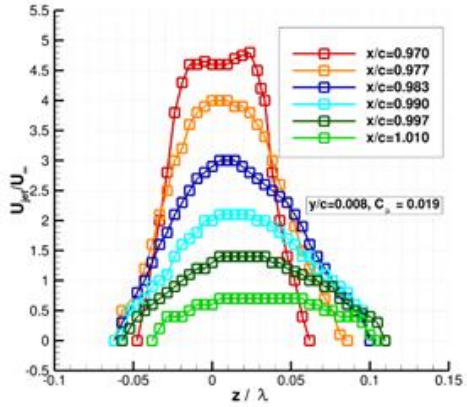

Figure 6. Streamwise velocity profiles as a function of the transverse position z/c at different streamwise positions x/c.

The velocity value is non-dimensionalised by the freestream flow of 10m/s chosen for the circulation control results presented further. Firstly, results show that the jet is slightly deviated in the transverse and vertical directions. According to the vertical direction, the center of the jet is displaced by only 1.4 % of λ in the downward y direction (Fig. 5). According to the transverse direction, the center of the jet is displaced up to 3 % of λ towards positive values of z (Fig. 6). Then, it is clear that the jet speed rapidly decreases with the streamwise direction. The velocity ratio $\frac{U_{jet}}{U_\infty}$ is equal to 4.5 at 2 jet diameters (or x/c = 0.965) and is equal to 2 at 14 jet diameters (or x/c = 1.005). Finally, by displacing the pressure probe in the spanwise direction at the maximum value of each jet exit velocity at x/d = 2 (with d the jet diameter), results exhibited a relatively low value of the standard deviation in the transverse direction of 13 %. As observed by Englar [15], the external flow field around the wing profile can have non-negligible effect on the jet flow. Therefore, it is probable that the jet behavior, in terms of spread and turning angle for instance, changes when the main flow is turned on.

3.4. 2D URANS simulations

The numerical approach was based on URANS simulations performed with the flow solver ISIS-CFD which is an incompressible unsteady Reynolds-averaged Navier-Stokes method mainly devoted to marine hydrodynamics. The solver is based on finite volume method to build the spatial discretization of the transport equations and the grids can be completely unstructured. The numerical simulations are 2D simulations. The computation domain starts 2c before the airfoil and extends 5c behind the airfoil. The height of the domain is 6c and the profile is centered in the domain. The mesh is generated using Hexpress, an automatic mesh generator and is then refined as explained in [16] and the minimum cell size is 0.1mm. This software generates meshes containing only hexahedrals. For the surface of the airfoil, a no-slip condition boundary condition is used and the wall normal resolution is $y^+ \leq 0.5$. The final mesh consists of 174809 for the angle of attack (AOA) of 5° (see Fig. 7). The turbulence model used in this study is the k - ω SST of Menter [17]. The actuation is implemented as boundary conditions. The velocity is imposed on the jet boundary as U = U_{jet} and the direction of the jet is perpendicular to the boundary.

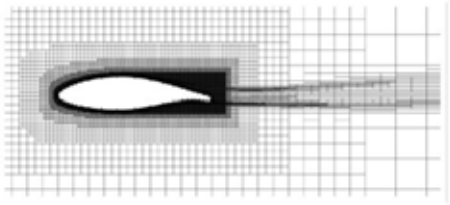

Figure 7. Refined mesh for an AOA of 5°.

4. RESULTS

4.1. Aerodynamic forces

For a Reynolds number of 2. 10^5, Fig. 8 shows the lift coefficient increment ΔC_L as a function of the angle of attack for both actuators with C_μ= 0.004 and C_μ= 0.019 for PA and SJD, respectively. These C_μ were chosen

because they provide similar lift gain at zero AOA where the lift coefficient is 0.5. When considering PA it seems that ΔC_L is constant with AOA, whereas ΔC_L appears to slightly increase with AOA for SJD. It is likely that SJD reenergizes the boundary layer for higher AOAs and then contributes to delay its incipient separation.

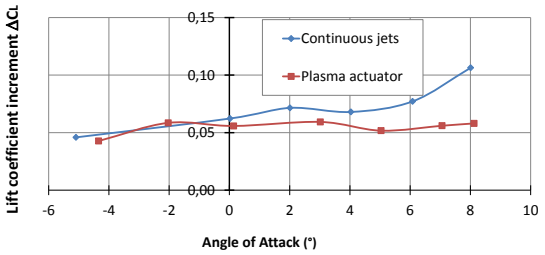

actuation versus angle of attack for both actuations.

Static pressure measurements are used to highlight the modification of aerodynamic forces with actuation. Due to the PA implementation at the trailing edge, pressure measurements close to the trailing edge are not available and were consequently performed with pressure taps implemented around the model between the leading edge and x/c = 0.7. Mean pressure distribution for SJD is obtained from an averaged value of static pressure in the transverse direction (z). Close to the jet orifice, no pressure tap was available (around x/c = 0.9).

In figures 9 and 10 the pressure distribution is plotted at U_∞ = 10 m/s without and with actuation. Slight differences can be observed on the wall static pressure distribution of the cases without actuation because of the different design and manufacture of both models and the selected AOA. Compared to the pressure distribution without actuation, the whole pressure distribution around the airfoil is modified for PA. Pressure distribution is slightly decreased on the suction side and increased at the pressure side.

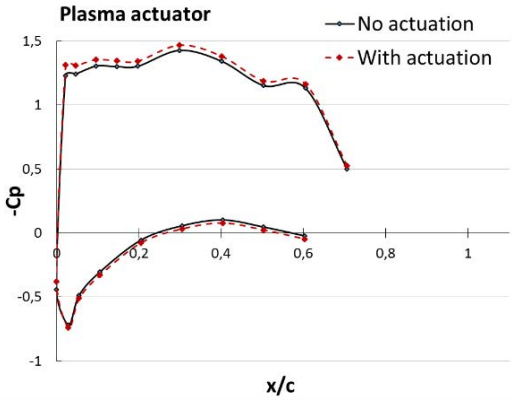

Figure 9. Wall static pressure distributions for PA, AOA = 5°.

With airfoil equipped with SJD, the same global trend is visible but it is completed by a local pressure suction peak at the trailing edge because the flow is accelerated by the momentum added by SJD. It is commonly observed in circulation control [15, 18].

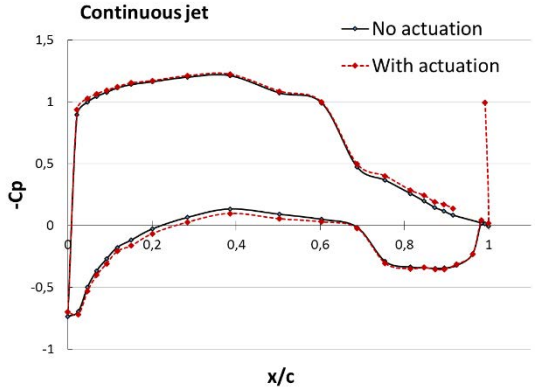

Figure10. Wall static pressure distributions for SJD, AOA = 4°.

4.2. Near wake

Figure 11 shows the natural flow around the airfoil trailing edge without actuation at an angle of attack of 5° and a Reynolds number equal to Re = 2. 10^5 by plotting mean time-averaged velocity contours and streamlines. It can be observed that the near wake, characterized by a recirculation zone due to the thick rounded trailing edge, develops on a length of 5% of the chord. Streamlines enable to highlight the two counter-rotating structures similar to the ones that can be observed at the base of bluff bodies.

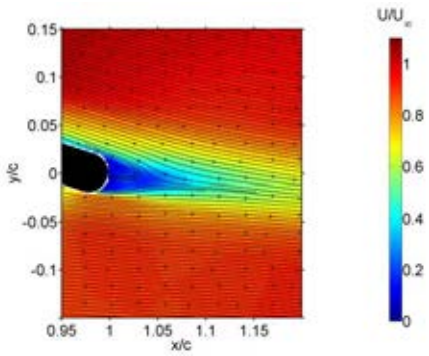

Figure 11. Topology of the baseline near wake in the centerline z = 0mm. Time-averaged streamwise velocity contours and streamlines.

Because of the 3D action on flow expected by SJD, the flow uniformity has been verified in the spanwise direction and is confirmed by the overlapping of the streamwise velocity vertical profiles drawn in the near wake in Fig. 12 and derived from PIV measurements.

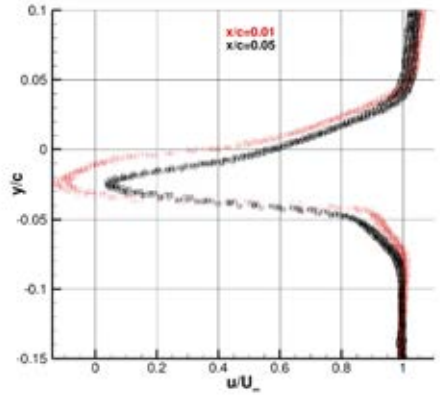

Figure 12. Overlapping of streamwise velocity profiles versus vertical direction for transverse positions z = -9, -7, -4, 0, 3, 7, 9 mm, plotted for two streamwise position x/c (SJD actuation).

Mean vertical velocity field contours and streamlines are plotted in Figs. 13 to visualize the modification of the near wake topology due to PA actuation. If no significant effects are measured for the streamwise velocity, the vertical velocity is reinforced by the actuation downward the trailing edge meaning that the wake is deflected towards the pressure side of the airfoil. This leads to flow circulation modification around the airfoil. For PA, the two counter-rotating structures are not suppressed whereas for SJD, their intensity and size are diminished as can be seen on Fig. 14 where mean streamwise velocity field contours and streamlines are plotted.

(a) No actuation

(b) With actuation C_μ= 0.004

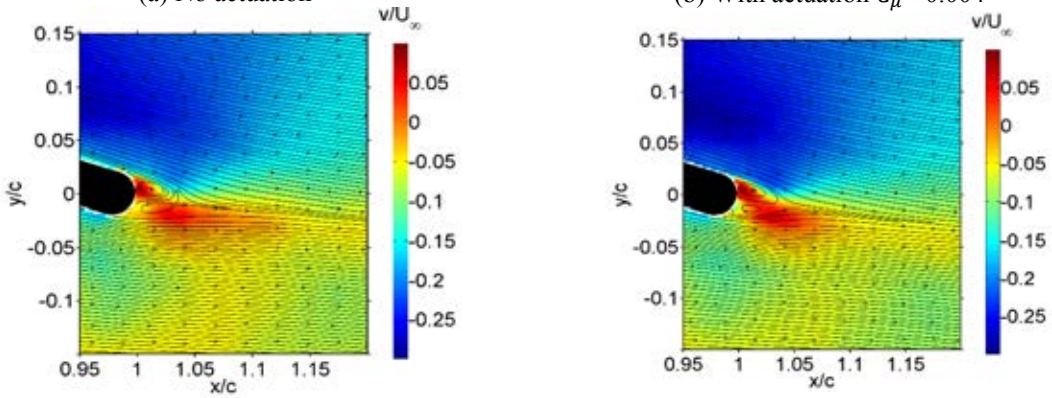

Figure 13. Vertical velocity field contours and streamline for the transverse section z = 0 mm (a) without and (b) with actuation for plasma actuation, Re = 2. 10^5, AOA = 5 °.

(a) No actuation

(b) With actuation - C_μ= 0.139

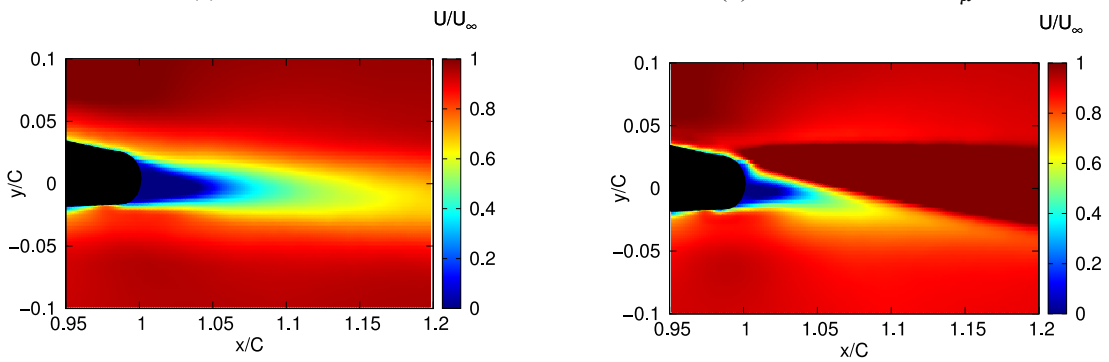

Figure 14. Streamwise velocity field contours and streamlines for the transverse section z = 0 mm (a) without and (b) with actuation for continuous jets, Re = 2. 10^5, AOA = 0 °.

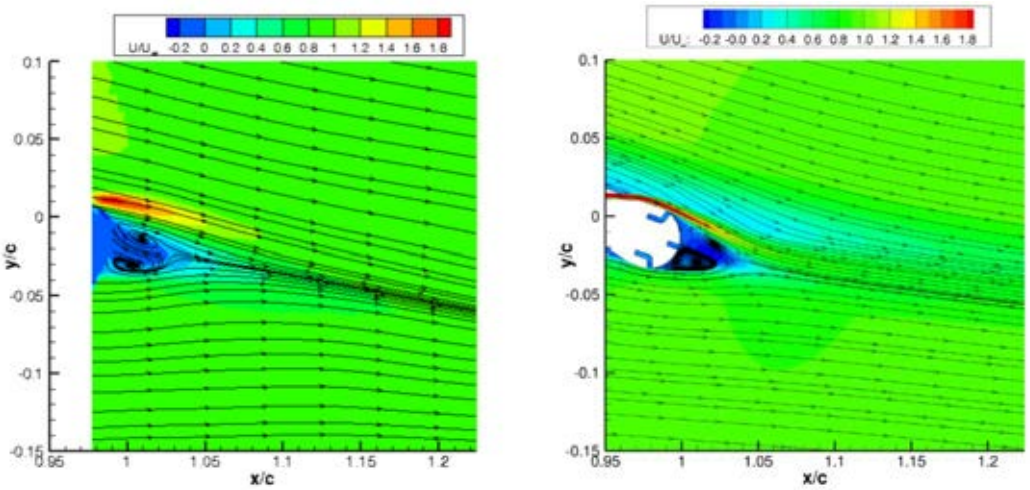

a) SJD (experimental tests) b) Slotted jets (numerical simulation)

Figure 15. Streamwise velocity field contours and streamlines for the transverse section z = 0 mm (a) for SJD (b) for slotted jets, C_μ= 0.027, Re = 2. 10^5, AOA = 5°.

In Fig. 15 is presented a comparison between velocity fields plotted in the near wake obtained for SJD or for slotted jets (numerical simulation) at iso C_μ= 0.027, leading to an increment of lift coefficient of 0.2 around. Remarkably, the peaks value of the streamwise velocity are approximately of the same order of magnitude $\frac{U}{U_\infty}$ = 1.8, while initial values of the imposed jet are different, $\frac{U_{jet}}{U_\infty}$ = 6 at for SJD and $\frac{U_{jet}}{U_\infty}$ is imposed to 2 in the hole of slotted jets. By looking more carefully on vertical profiles at two streamwise distances, the slotted jet exhibit a significantly different mean shear than the discrete squared jets. Indeed, the peak width of the streamwise velocity is much thinner in the slotted configuration, and is accompanied with a much stronger deceleration in the positive y/c direction.

Figures 16 and 17 zoom in on streamwise velocity profiles in the near wake at the streamwise location x/c = 1.05 in the recirculation area. It can be observed a change of the recirculation area due to the actuation. For PA, the maximum streamwise velocity deficit slightly moves downward, establishing the wake deflection due to the plasma actuation. For SJD, the action is much stronger, with the introduction of local high shear at the jet location. As for PA, the displacement of the minimum velocity towards negative y values is also evident. This proves that the lift gain obtained with both techniques is clearly obtained through a modification of the circulation around the wing.

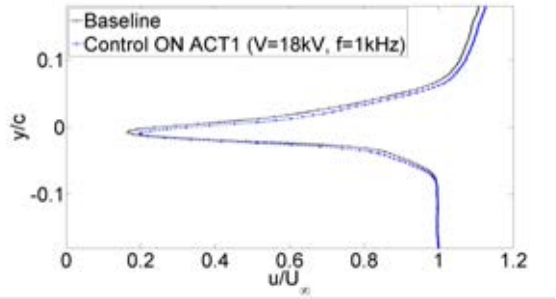

Figure 16. Time averaged streamwise u-velocity component versus y/c at x/c =1.05 for PA actuation. Re = 2. 10^5, AOA = 0 °.

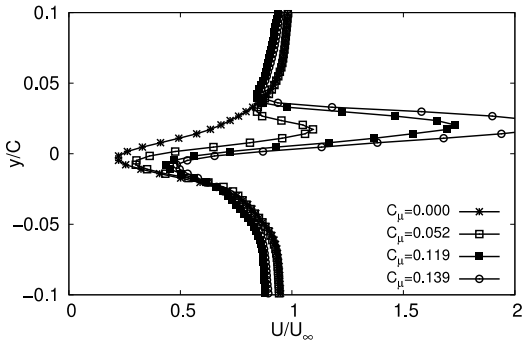

Figure 17. Time averaged streamwise u-velocity component versus y/c at x/c =1.05 for SJD actuation, Re = 2. 10^5, AOA = 0 °.

Focusing on 3D effects of SJD, Fig. 18 shows an average streamwise velocity field taken at x/C=1.01 behind the profile for C_μ= 0.119. The recirculation area limits are indicated as the zero velocity white line. As can be seen the SJD actuation locally pinches the recirculation area. Hence, the circulation control by slotted jet shows limited effect in the spanwise direction.

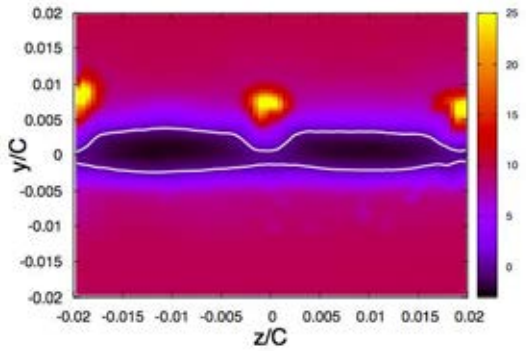

Figure 18. Average streamwise velocity field taken at x/C = 1.01 for C_μ= 0.119, AOA = 0°.

In Fig.19 is presented the zero velocity isoline obtained for different injection coefficient taken at x/c = 1.01. The effect of SJD actuation is clear is this figure: it progressively pinches the recirculation area. The recirculation zone can even be cut it into parts, which has the effect of creating cells of negative streamwise velocity. The role of these cells is not clear at this point on the lift gain, but it is likely that imposing such a spanwise wavelength may have a strong impact on the wake instability.

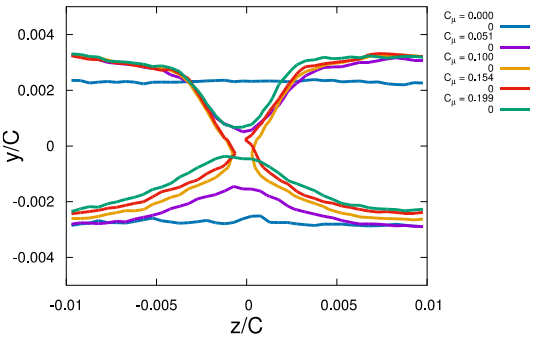

Figure 19. Zero velocity isoline geometry for various injection coefficient taken at x/c = 1.01 for Cμ= 0.119, AOA = 0°.

5. CONCLUSION AND PERSPECTIVES

This study presented the first results in analyzing lift increase achieved by different methods of active flow control acting at a rounded trailing edge of a realistic modified 2D wind turbine blade (NACA654-421 profile) with the objective to alleviate loads due to atmospheric flow conditions. Two control techniques were implemented experimentally, namely a plasma configuration and a discrete squared jet configuration. A configuration with a slotted jet was studied from 2D numerical simulation.

Investigation in terms of lift gain and mean spatial organization in the near wake were performed. They allowed lift increase monitoring by involving different mechanisms of interaction with the natural flow. DBD actuators and slotted jets are supposed to act as a bi-dimensional wall jet and squared jet distribution has a three-dimensional action on the flow. A lift increment up to 0.3 around could be obtained by jet configurations according to different momentum coefficients whereas the lift gain was limited to 0.08 by plasma actuators. It was also found that only the discrete squared jet configuration was able to completely suppress the flow separation on the side of the controlled jet. Future work will perform 2D simulations to compare plasma actuation with experiments and 3D simulations to compare the discrete squared jet configuration with experiments as well. This will help to remove the doubt on how to generate realistic controlled jets numerically and will provide a useful tool to investigate a distributed control action.

6. ACKNOLEDGMENTS

This present work is partly funded by the national French project SMARTEOLE / ANR-14-CE05-0034.

7. REFERENCES

1. Joslin, R. D., and Jones, G. S., (2006). Progress in astronautics and aeronautics 214 AIAA Inc.

2. Kweder, J., Panther C. C. and Smith, J. E. (2010). Int. J. Eng (4), pp411–429.

3. Dumitrache, A., Frunzulica, F., Dumitrescu, H., Cardos, V. (2014). Incas Bulletin (6) 2, pp33 – 49, ISSN 2066 – 8201.

4. Johnson, S. J., Case van Dam, C.P. and Berg, D. E. (2008). Active Load Control Techniques for Wind Turbines SANDIA Report.

5. Zhang, P. F., Yan, B., Liu, A. B. and Wang, J. J. (2010). AIAA Journal (48) 10.

6. Kotsonis, M., Pul, R. and Veldhuis, L. (2014). Exp. in Fluids (55):1772.

7. Compton, D. and Johnston, J. (1992). AIAA Journal (30).

8. Cathalifaud, P., Godard, G., Braud, C. and Stanislas, M. (2009). Journal of Turbulence (10) 42.

9. Laval, J., Braud, C., Fournier, G. and Stanislas, M. (2010). Journal of Turbulence (11).

10. Cuvier, C., Braud, C., Foucault, J. and Stanislas, M. (2011). 7th Turbulence And Shear Flow Phenomena, Ottawa-Canada.

11. Aubrun, S., Leroy, A., Devinan,t P. (2015). Proc. in 50th 3AF International Conference on Applied Aerodynamics, Toulouse, France, March 29-30 – April 01.

12. Taylor, Z. J., Gurka, R., Kopp, G. A. and Liberzon, A. (2010). IEEE Trans. on Instrumentation and Measurement (59) 12, pp3262-3269.

13. Sosa, R., Artana, G., Moreau, E. and Touchard, G. (2007). Exp. in Fluids (42), pp143–167.

14. Englar R. J., (1975). Subsonic Two-Dimensional Wind Tunnel Investigation of the High Lift Capability of Circulation Control Wing Sections. ASED-274, April 1975.

15. Englar R. J. (1975). Experimental investigation of the high velocity coanda wall jet applied to bluff trailing edge circulation control airfoils. Technical report, DTIC Document, 1975.

16. Braud, C. and Guilmineau, E. (2016). Journal of Physics: Conference Series 753 (2016) 022031, presented in TORQUE 2016, October 5-7, Munich, Germany.

17. Menter, F. (1994). AIAA Journal 32, pp1299-1310.

18. Jones, G. S., Viken, S. A., Washburn, A. E., Jenkins, L. N. and Cagle, C. M. (2002). AIAA paper, 3157(1).